URANSE simulation of an active variable-pitch cross-flow Darrieus tidal turbine : sinusoidal pitch function investigation

B. Paillard, J.A. Astolfi, F. Hauville

PII: S2214-1669(15)00014-4
DOI: http://dx.doi.org/10.1016/j.ijome.2015.03.001
Reference: IJOME 52

To appear in:

Received Date: 9 December 2014
Revised Date: 13 March 2015
Accepted Date: 25 March 2015

Please cite this article as: B. Paillard, J.A. Astolfi, F. Hauville, URANSE simulation of an active variable-pitch cross-flow Darrieus tidal turbine : sinusoidal pitch function investigation, (2015), doi: http://dx.doi.org/10.1016/j.ijome.2015.03.001

URANSE simulation of an active variable-pitch cross-flow Darrieus tidal turbine : sinusoidal pitch function investigation

B. Paillard[a], J.A. Astolfi[a], F. Hauville[a]

[a] *Mécanique et Energétique en Environnement Naval (M2EN), Institut de Recherche de l'Ecole Navale (IRENAV) BCRM Brest, ECOLE NAVALE ET GROUPE DES ECOLES DU POULMIC - IRENAV, CC 600 29240 BREST Cedex 9 France*

Abstract

This article describes a 2D CFD simulation implementation of a crossflow tidal turbine, the blades of which have their pitch modified during revolution. Unsteady flow around the turbine is computed with an URANSE method, using the solver ANSYS-CFX. Spatial and temporal discretizations have been studied. The pitch motion of the blades is obtained through mesh deformation, and the main rotation is implemented through sliding boundaries, with general grid interface model. The turbulence model used is kω SST. Langtry Menter transition model was tried but showed high discrepancies with experimental results. Five experimental cases were used to assess the accuracy of the simulation. It provided accurate computed forces for a wide range of tip speed ratios, and proved to be suitable for exploratory simulations. Harmonic pitch control was thus implemented for a tip speed ratio of 5, close to an operational value for a crossflow turbine. First, second and third harmonics pitch function were tested. It was shown that an improvement of more than 50% could be achieved with the second harmonics, with a large reduction in thrust. The flow inside the turbine and close to the blade was examined so that the case of performance improvement due to pitch control could be clearly understood. It was observed that turbine efficiency improvement requires a very slight recirculation and an angle of attack decrease on the upstream part of the turbine, and an angle of attack increase on the downstream part. The flow deceleration through the turbine was found to be a primary factor in pitch function as well. Moreover the hydrodynamic torque and thus the energy required to control the pitch were found to be insignificant.

Keywords: Darrieus, Variable pitch, Dynamic Stall, URANSE

1. Introduction

Tidal turbines are a power source that shows many significant advantages over other solutions [1]. No land is occupied unlike a dam, there is a steady predictable power output unlike with wind turbines, and low waste or side effects are generated unlike fossil fuel or nuclear power plants. These devices can consist of a classic horizontal axis systems, or cross-flow turbines which have many advantages in water : rectangular surface area helps increasing power production in shallow locations, fixed pitch devices can operate in any flow direction [2] and centrifugal loads, which evolve with ω^2, are less severe than in air [3]. Variable pitch cross-flow turbines enable a Darrieus system to improve its performance and decrease radial forces, which do not generate a torque and are responsible for fatigue and system failure [4]. They have been studied at IRENAV since 2007 as a part of the SHIVA project, which aims at the implementation of an experimental variable pitch crossflow tidal turbine [5, 6, 7]. This device has cantilevered blades and its arms are not submersed, thereby cancelling parasitic arm drag.

The optimization of the pitch variation is of prime concern in order to take full advantage of the added mechanical complexity required to obtain these kinematics. However the complexity of the flows associated with these devices requires to choose and check the simulation tools with great care. A stream tube model coupled with the ONERA-EDLIN dynamic stall model was developed [8]. However it does not give precise information on the pattern of the flow associated with each pitch function used. Furthermore these empirical dynamic stall models are limited to the applications they were calibrated for. Finally, the stream tube model is relevant for design and overall performance assessment, but the forces and local phenomena predicted

Email addresses: ben.paillard@gmail.com (B. Paillard), jacques-andre.astolfi@ecole-navale.fr (J.A. Astolfi), frederic.hauville@ecole-navale.fr (F. Hauville)

c, l, r, N	turbine chord, span, radius and number of blades	m
C_n, C_t	normal and tangential force coefficients, $C_{n/t} = \frac{F_{n/t}}{\frac{1}{2}\rho c l v_r^2}$	/
	the tangential force creates torque and is the useful part of the hydrodynamic force	
	the normal force creates no torque	
η	power coefficient, $\eta = \frac{\text{power}}{\frac{1}{2}\rho 2rlv_\infty^3}$	/
C_p	pressure coefficient, $C_p = \frac{p-p_\infty}{\frac{1}{2}\rho v_r^2}$	/
N	turbine number of blades	/
Re	chord Reynolds number, $Re = \frac{r\omega c}{\nu}$	/
S_{blade}	blade surface, $S = cl$	m^2
$S_{turbine}$	turbine surface, $S = l2r$	m^2
v_r	relative flow velocity $v_r = v_\infty\sqrt{\cos(\theta)^2 + [\sin(\theta) + \lambda]^2}$	m/s
v_∞	upstream flow velocity	m/s
α	incidence	rad
λ	tip speed ratio $\lambda = \frac{r\omega}{v_\infty}$	/
ω	rotational velocity	rad/s
σ	system solidity, $\sigma = \frac{Nc}{2r}$	/
θ	main angular position	rad

Table 1: Nomenclature

remain questionable [9]. Being able to accurately compute the unsteady forces is mandatory in order to optimize the pitch function, which is why a RANSE simulation was developed.

The purpose of the present work is to implement and validate a 2D RANSE simulation of a lifting foil undergoing a Darrieus kinematic, without pitch variation. The quantities of specific interest are the forces and torques applied to the blades, and the flow around the whole system. It is the preparatory work to the development of the variable pitch cross-flow turbine simulation. First the computation methods used are introduced in comparison with the previous existing references. Then the simulation parameters and discretizations are studied and chosen, and will be used as a basis for future works. The results from the numerical simulation are then verified against experimental results from bibliographic references. Finally the flow field and pressure coefficient curves are discussed, in order to give a better insight to the reader on the flow physics.

The purpose of the present work is to present the implementation of a 2D unsteady RANSE simulation of a lifting surface undergoing two simultaneous motions : a Darrieus kinematic, which is a rotation around a point away from the foil ; and a dynamic pitch control, defined as a rotation around the quarter chord, adapting the angle of attack of the lifting surface to the local flow state. This second kinematics is aimed at performance improvement and radial forces reduction. The quantities of specific interest are the forces and torques applied to the blades, and the flow around the whole system.

2. Material and methods

2.1. Bibliographic background

Cross-flow turbines feature complex fluid phenomena, and have first been studied using momentum based models for overall performance prediction. These models cannot predict local flow accurately, and can fail in unsteady forces prediction. Unsteady CFD appeared as a good solution to overcome these limitations. First computations of this kind were implemented for cross-flow turbines in the late 1990's. Various recent projects are being carried out in this area. Allet and Paraschivoiu [10] simulated a 2D one blade turbine with NACA 0015 section. The governing equations were solved by the streamline upwind Petrov-Galerkin finite element method. Turbulence effects were introduced in the solver by the algebraic Cebeci-Smith model (CSM) and the non-equilibrium Johnson-King model (JKM). The forces oscillations were in agreement with the experimental results, even though the extremum values and some vorticity shedding could not be reproduced. Ferreira [11] compared PIV measurements with several types of CFD models : LES, DES and RANSE, combined with several turbulence models. The best model was found to be the DES model. The spatial grid did not enable the LES model to give correct results in the boundary vicinity. Consul et al. [12] assessed the influence of solidity on performance. Turbulent models Spallart-Allmaras and $k-\omega$ SST were compared, and the latter was found to be more accurate. Qualitative agreement with experimental

results were obtained. Klaptocz et al. [13] used Spallart-Allmaras model to simulate a turbine fitted inside a diffuser. The turbine was modelled using a rotating ring. Comparison with experiment is poor for local forces, but global efficiency curves are obtained accurately. An innovative hybrid RANSE/momentum model was studied by Antheaume et al. [14]. The global flow through the turbine is simulated with a RANSE model, and the local influence of the blades on this flow is computed with a stream tube model. It finds its application mostly on farm modelization.

Variable pitch crossflow turbines can be divided into two categories. Active pitch controls are devices for which the pitch angle function is constant during operation, but can be changed through a controller when operating conditions change. Passive pitch controls are devices for which azimuthal position and rotational velocity have an impact on the pitch function, often implemented through mass-spring arrangements [15]. The former will be studied in this paper. Several experimental projects have been carried out to evaluate the use of variable pitch on crossflow axis turbines. Miau et al. [16] compared starting torques for 70° and 10° maximum pitch amplitude. With 70°, a higher starting torque was reached, but a higher efficiency in operation was anticipated numerically for 10°. Hwang et al. [17] studied a cycloidal turbine similar to Pinson turbine, for which a cam and an eccentric were used, yielding a quasi-sinusoidal pitch function. A power coefficient of 0.25 was achieved. Grylls et al. [18], Nattuvetty et al. [19] and Erickson et al. [20] also tested numerically and experimentally a device similar to Pinson turbine including a pitch offset, and could reach a η of 0.45. The company McDonnell tested a variable pitch wind turbine [21], for which the pitch law was optimized numerically beforehand, and implemented by manufacturing the corresponding cam track. They obtained a maximum η of 0.39. Vandenberghe et al. [22] studied a device similar to Pinson turbine, with a second order harmonic pitch control. Asymmetric pitch law could thus be obtained, in order to adapt the pitch to the reduced velocity encountered downstream. They reported a gross maximum experimental η of 0.436, after arm drag and control loss subtraction. First order harmonic was still best for λ above 3. Finally the company WPI studied an individual pitch control device [23]. A performance coefficient of 0.5 was measured experimentally at NTNU. It should be noted that the holding arms of this turbine are outside of the water. This effectively cancels arm drag, which can be as high as .25 points of Cp. The same configuration will be used SHIVA experimental platform.

The RANSE solver CFX was chosen because of the previous works on unsteady forces simulation on NACA foils at IRENAV [24]. The various simulations that had been implemented were considered a valid and strong basis for such a demanding flow simulation. The complexity and accuracy of $k-\omega$ SST model were seen as a valid step between the faster but less physically accurate DMST [8], and future work with more complex fluid models such as DES or LES.

2.2. Experimental reference

Two sources were considered for validation [25, 26]. Both experimental devices were straight blades, fixed pitch Darrieus turbines, with their blades connected at the quarter chord. Various solidities and λs were considered, enabling a thorough validation process. The data are gathered in table 2. Cases 1, 2 and 3 were carried out in a towing tank, hence the very low flow velocity.

These results were chosen because local blade loads were measured, which gives a more accurate validation than averaged values such as the coefficient of performance. To the best knowledge of the author, there exist no more recent publications, or pitch-controlled cases of local blade loads measurement on crossflow axis turbines. Such an experimental device is under construction at IRENAV [7]. Even though both experimental campaigns were carried out around $Re = 4.10^4$ which is relatively low, they are relevant since they cover a wide range of tip speed ratios including an operational one. No detailed experimental data could be found for higher Reynolds numbers, at which full scale turbines will operate. No uncertainty quantification on forces measurement were provided in these articles. Blade deformation, calibration and alignment uncertainty, probes accuracy were not mentioned. Furthermore, the tangential force is an order of magnitude lower than the normal force, which makes its measurement accuracy even more questionable. However theses results are the most detailed available at the time this article was written. Two separate campaigns were considered in order to reduce as much as possible such uncertainties.

The measured quantities in this study are the normal and tangential force coefficients defined by equations $C_n = F_n/\frac{1}{2}\rho clV_\infty^2$ and $C_t = F_t/\frac{1}{2}\rho clV_\infty^2$. The tangential force generates torque, whereas the normal force does not. Hence they are relevant in the study of cross-flow turbines since they are respectively the non-productive and the useful forces for torque production. The coordinate system used is defined in figure 1. The turbine rotates in anti-clockwise direction. Angular datum is the position of the blade when it leaves downstream part and enters upstream.

	Case 1	Case 2	Case 3	Case 4	Case 5
fluid		water		air	
upstream fluid velocity	0.183 m/s	0.091 m/s	0.061 m/s	3.2 m/s	6.4 m/s
blades number		2		2	1
rotor diameter		1.22 m		0.61 m	
span		1.1 m		0.61 m	
chord		0.0914 m		0.061 m	
solidity		0.15		0.2	0.1
blade section		NACA0012		NACA0018	
rotational speed		43 rpm		300 rpm	
λ	2.5	5	7.5	3	1.5
chord Reynolds number		4.10^4		$3,80.10^4$	
η	0.077	0.362	-0.022	-0.129	-0.018
source		[25]		[26]	

Table 2: Experimental cases used in this article

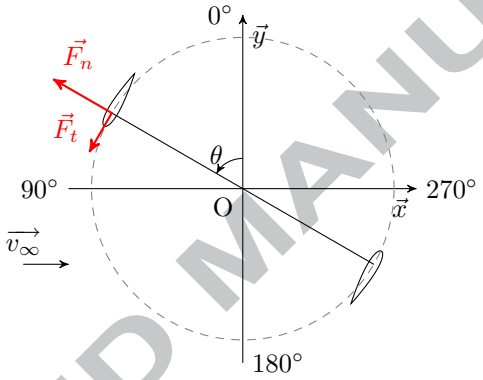

Figure 1: Coordinate system used for the present study

2.3. Numerical procedure

2.3.1. Simulation configuration

The commercial RANSE solver CFX is used for this simulation. A ring rotating at constant speed is enclosed inside a steady domain, as shown in figure 2. The flow across the non-conformal boundaries is obtained with a general grid interface or GGI [27]. A 2D approach is relevant for both experimental cases, since the aspect ratios are 12 for cases 1, 2 and 3 ; and 10 for cases 4 and 5, and the blades were positioned as close as possible from the wall of the experimental infrastructure used, thereby cancelling finite wing effect ; and the arms loss were cancelled by keeping the holding arm outside of the water in [25], and reduced using a single streamlined arm together with strings in [26]. The low λ used in the latter contribute to further arm loss reduction. Progressive start of the rotating domain was tested, but no difference in forces and torque with step start could be observed after one revolution. The domain is 10 turbine diameters in the transverse direction, 3 diameters upstream and 10 diameters downstream. The inlet condition is a fluid velocity on axis x. The tip speed ratio considered defines the norm of this velocity vector, since the rotational velocity remains constant. The inlet turbulence rate is fixed at 5%. Outlet condition is defined with a relative pressure equal to 0 Pa. For the streamwise boundaries a symmetry condition is used. Finally the blades are defined by a solid no slip boundary condition. The spatial resolution scheme used is a second order Euler method, and the temporal scheme is a second order backward Euler method. The implicit form of the solver does not impose any numerical limitation on the Courant number value. However the physical problems associated with Darrieus kinematics requires a small enough time step in order to accurately resolve transient flow details. This is studied in part 2.3.3. Convergence is measured through residual RMS, for which criterion is 10^{-4}.

nr. of elements	$\overline{V/V_\infty}$	rel. difference
200 000	0,536	14,50%
300 000	0,471	0,64%
400 000	0,468	-

Table 3: Relative difference in flow deceleration for several spatial discretization, case 2, $\lambda = 5$

2.3.2. Spatial discretization

A rotating ring inside a steady domain was used. The meshing is structured in the outside domain and in the ring, and unstructured, tet-dominant in the center part. An O-grid technique was used around the foils, and the ring width was set to 3 chords so that the mesh can deform smoothly during pitch variation, and the high gradient around the blades are kept away from the sliding interfaces. Mesh spacing continuity across the interfaces ensured an accurate simulation across them. For the boundary layer discretization, conclusions on mesh study from Ducoin [24] were used. 40 cells were used for boundary layer thickness, and 300 cells in the chordwise direction. First cell size was adapted to the experimental cases in order to account for diameter and flow differences. The dimensionless wall distance $y+$ was always kept below 1 in order to compute viscous layers accurately. A convergence study on spatial discretization was carried out. Three different meshes were built, including respectively 200 000, 300 000 and 400 000 elements. Flow at turbine center divided by inlet flow is the quantity used as the convergence criteria, in order to accurately measure the upstream-downstream interaction. Mesh independence is obtained for 300 000 elements. Table 3 shows the results for case 2. The final mesh consists of 50 000 cells in the center, 100 000 in the outer part, 150 000 in the ring.

The blades pitch angles are changed over time. Previous studies implemented that feature through rotation of circular regions enclosing each blades [17]. Another GGI method was then used. In the present study this is obtained through mesh deformation in the ring containing them. The solver deforms the mesh at every time step. The mesh is treated as a deforming structure, with rigidity increasing with smaller cell size, so that the small cells in the boundary layer remain undeformed. An Arbitrary Lagrangian-Eulerian (ALE) formulation is used to solve the motion of the mesh. The Lagrangian deformation enable easy and precise boundary and interface conditions, but may create severe mesh distortion. On the other hand Eulerian deformation creates no distortion, but solid boundary and interfaces are difficult to apply, since boundary and mesh nodes do not necessarily coincide. With the ALE approach both technique are used in a single domain, so that boundaries can be precisely tracked, and cell quality can be optimized away from them. The motion of each node is taken into account by modifying the conservation equations. The control volume changes over time, and the velocity of its boundaries is used in the ALE formulation. An illustration of the meshing strategy and deformation can be found in figure 2.

2.3.3. Temporal discretization

The time step is controlled through the angular step since rotational velocity is constant. The following azimuthal steps were tested : 0.5°/step, 1°/step and 2°/step, which gave CFL-RMS values of 3, 5 and 10 respectively. The forces coefficients do not change below an angular step of 1°. This value will be used in the following study. The results for case 4 after 9 revolutions can be found figure 3.

2.3.4. Wake survey

An accurate description of the impact of upstream part on downstream part requires a fully developed turbine wake. For 3 different experimental cases the evolution of tangential force was inspected for convergence as the wake develops. The results are shown in table 4. The wake became fully developed for all cases at the ninth revolution. This value will be used in further study. The number of revolutions required increases with λ. Higher λ leads to faster rotation, hence less time per revolution for the wake to convect.

2.3.5. Turbulence modelization

The low chord Reynolds number and the unsteadiness of the flow raise questions about the choice of turbulence and transition models. A Large Eddy Simulation (LES) or Detached Eddy Simulation (DES) model has shown better results for Darrieus turbine simulation at the cost of longer computation time [9]. However this work aims at the optimization of a pitch angle function, which will require many cases to be considered. DES is at least one order of magnitude more computer intensive than RANSE models [27], which makes the cpu time prohibitive for our goal. Furthermore this study was carried out in 2D, whereas DES and LES were developed to simulate the 3D nature of turbulence. Even though promising results were

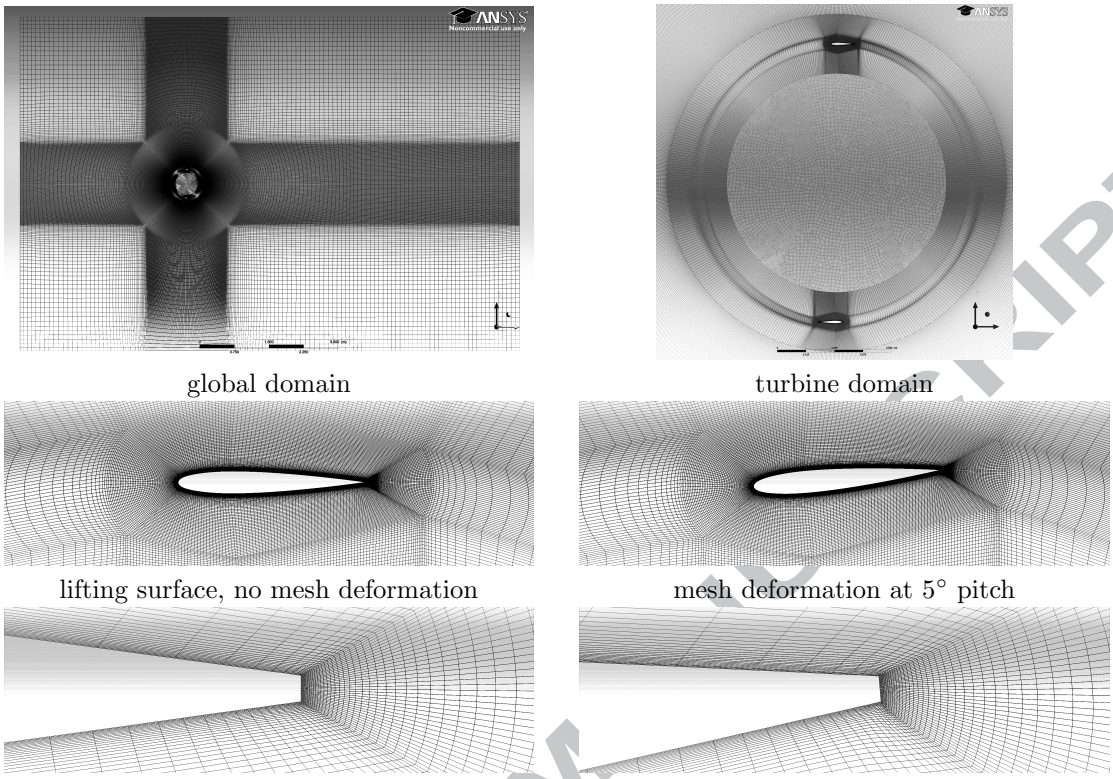

Figure 2: General meshing configuration

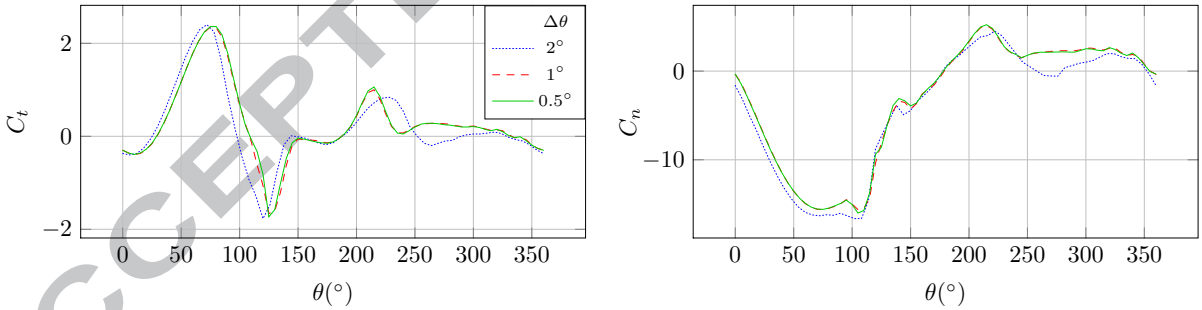

Figure 3: C_t and C_n for case 4 ($\lambda = 3$) as a function of angular position for three angular steps ($\Delta\theta = r\Delta t$)

revolutions	case 1	case 2	case 3
5	1,34%	6,40%	8,03%
6	0,56%	4,11%	5,03%
7		2,50%	3,14%
8		1,33%	1,83%
9		0,54%	0,82%

Table 4: Relative tangential coefficient variation with wake development for cases 1, 2 and 3

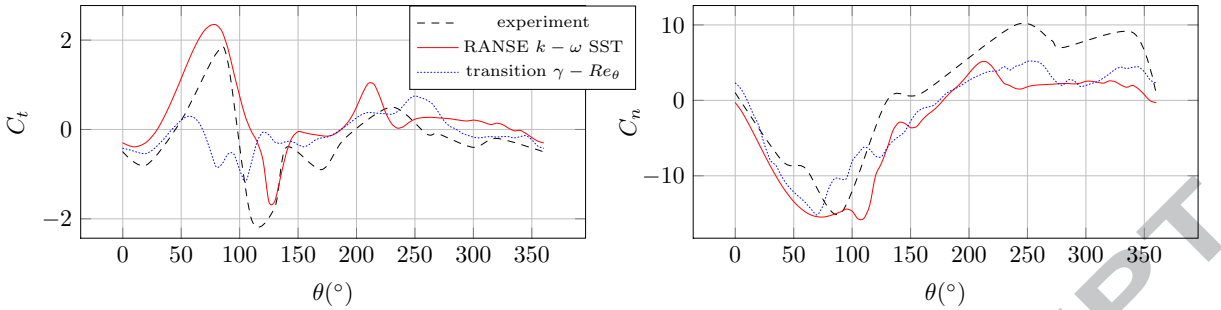

Figure 4: C_t and C_n for case 4 ($\lambda = 3$), with/without transition model

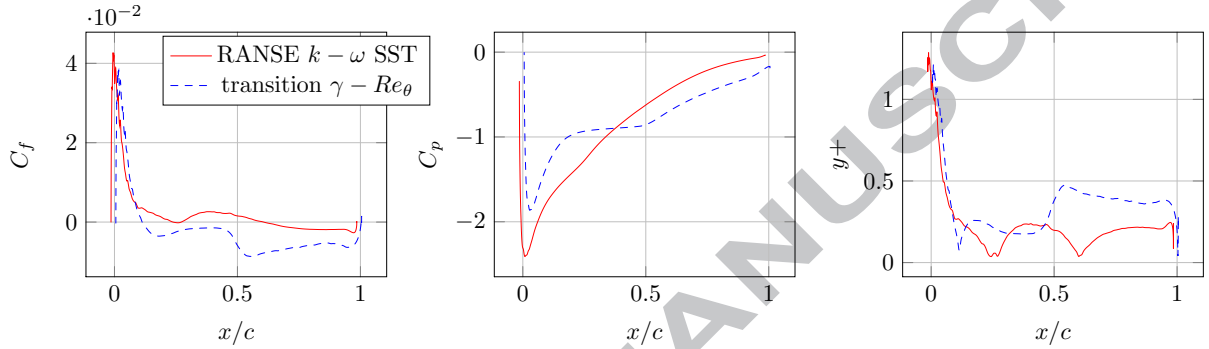

Figure 5: Pressure, friction coefficients and y+ parameter for case 4 ($\lambda = 3$) at $\theta = 50°$

obtained using LES or DES in 2D when compared to RANSE and 3D LES or DES [9], [28], it was decided not to use it for the present study. The turbulence model used in this study is $k-\omega$ SST, which combines $k-\omega$ model close to boundaries and $k-\epsilon$ in further domain, with blending functions between them. It is a two equation model, which showed good results on solid boundary flows involved in cross-flow turbines simulation [29].

Transition from laminar to turbulent boundary layer [30] can have a very strong influence on flows around lifting surfaces. It can improve performance by delaying separation [31], and it can degrade it when a separation bubble occurs [32]. $\gamma - Re_\theta$ transition model was tested [30, 33]. It simulates transitional behavior by comparing a local Reynolds number to a reference value Re_θ correlated experimentally, and by using an intermittency number γ. Fully turbulent $k-\omega$ SST and turbulent with transition $\gamma - Re_\theta$ model were compared in the present study. Force results from simulation of case 4 are given in figure 4. Unlike numerical results, experimental normal force coefficient between 0° and 90° does not decrease steadily, as should be anticipated from a constant incidence increase. This is a typical result during laminar separation bubble formation [34]. However the transition model could not reproduce it, and an early stall is simulated on the upstream part, clearly visible on C_t curve.

Friction and pressure coefficients C_f and C_p, and y+ are shown in figure 5 for $\theta = 50°$. Transition model reaches a negative C_f value at 0.1c, and C_p curve has a plateau, two signs of stall onset. y+ curve rise steeply at 0.5c which shows the transition onset. This leads to the conclusion that laminar stall is predicted by the transition model, unlike what the experimental results show. The inlet turbulence rate has a strong influence on the transition model behaviour and has not been studied here. Stall consequences are over predicted with the transition model, which leads to the choice of the turbulent $k-\omega$ SST model in the following study. The transitional flow remains an important phenomenon for this range of Reynolds number. Numerical and experimental testing is currently being carried out at IRENAV on that topic [35]. The first results show an important influence of the laminar separation bubble on transition and stall, which might explain the early stall computed by the model (figure 4).

3. Results and discussion

3.1. Validation

Comparison with experiments on force coefficient is studied in this section. Figure 6 shows the results for case 1, which is close to where most crossflow axis turbines usually operate. Agreement is average. An

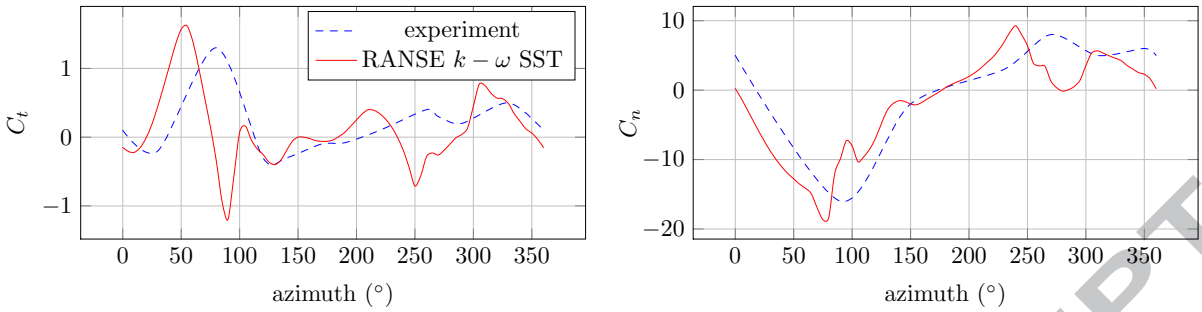

Figure 6: Validation on C_t and C_n for case 1 ($\lambda = 2.5$, $\sigma = 0.15$)

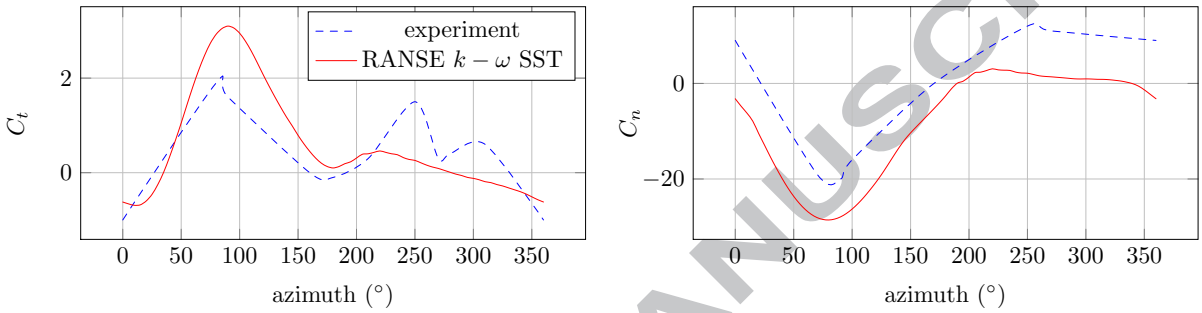

Figure 7: Validation on C_t and C_n for case 2 ($\lambda = 5$, $\sigma = 0.15$)

angular offset is observed which could be explained by a slight blade misalignment. Stall is predicted early and stronger. A large C_t drop at $\theta = 90°$ is predicted, a sign of a deep stall, not observed experimentally. Numerical and experimental turbines thus operate in complete different conditions at that azimuth. This is the only case where such a difference occurs. It can be noted that with λ and solidities of 3 and .2 respectively for case 4, experimental stall is observed (see figure 9). Reducing solidity creates less flow blockage and thus less flow deceleration ; and lower λ gives a higher incidence. These characteristics increase stall inception, and one should then expect case 1 to exhibit stall as well. A blade roughness difference between the experimental sources can be incriminated. The dynamic stall modelization and transitional behaviour are also questionable. Further numerical testing are currently being carried out at IRENAV.

Case 2 is shown in figure 7. Computed upstream C_t is 50% higher than measurements. In the downstream region, numerical C_t remains very low compare to the experiment. C_n results show an offset as well. The discrepancies can be due to a slight misalignment of the blade pitch in the experiments as suggested by similar results obtained by [9, 36, 37] where Darrieus turbine for different conditions of pitch and pitching axis where studied. It was observed that a small pitch misalignment can create such a deviation. Indeed when the foil is pitched nose-out the incidence decreases upstream and increases downstream, which changes the tangential force and normal forces as described above. Numerically, an inaccurate estimation of upstream/downstream interaction can be incriminated. Spatial discretisation study showed that further wake refinement did not increase accuracy. That phenomenon is currently under investigation at IRENAV.

Case 3 is shown in figure 8. In that case the agreement is fairly good, particularly in the upstream part of the turbine. The upstream C_t peak is well reproduced. However discrepancies are observed in the downstream part. Experimental oscillations originating probably from stall vortices.are observed in the experiments were not simulated. In the same manner as case 2, it can be argued that the influence of the upstream part on the downstream part is not accurately reproduced.

Case 4 is shown in figure 9. The agreement is fairly good. The evolution is well reproduced showing the ability of the model to account for the unsteady stalled behaviour of a Darrieus turbine at low λ.

Case 5 is shown in figure 10. This case involves large incidence variations and deep stall. The agreement is very good. C_t oscillation frequency is reproduced accurately, and the amplitudes differs of about 10 to 20%. The simulated C_n oscillates more than the experimental results, but the mean values are close. These oscillations are due to stall vortices convected along the chord. For both coefficients, the simulation is more accurate in the upstream part where angle of attack is large, showing the ability of this model to simulate deep stall. Again discrepancies are observed rather in the downsteam part of the turbine.

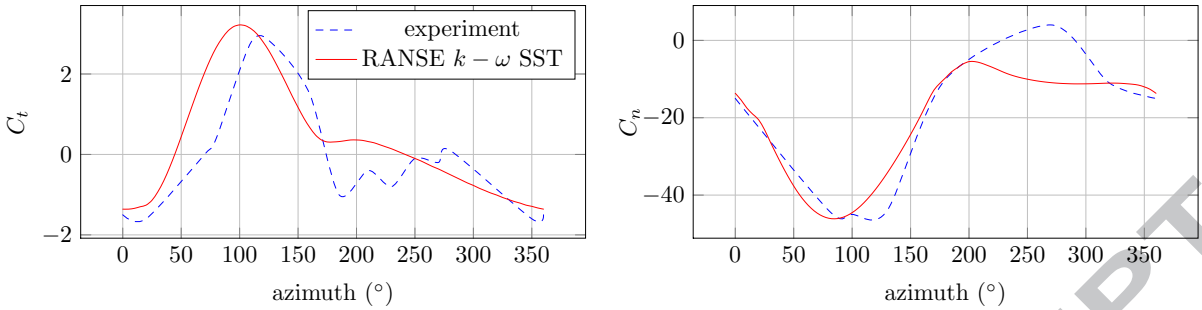

Figure 8: Validation on C_t and C_n for case 3 ($\lambda = 7.5$, $\sigma = 0.15$)

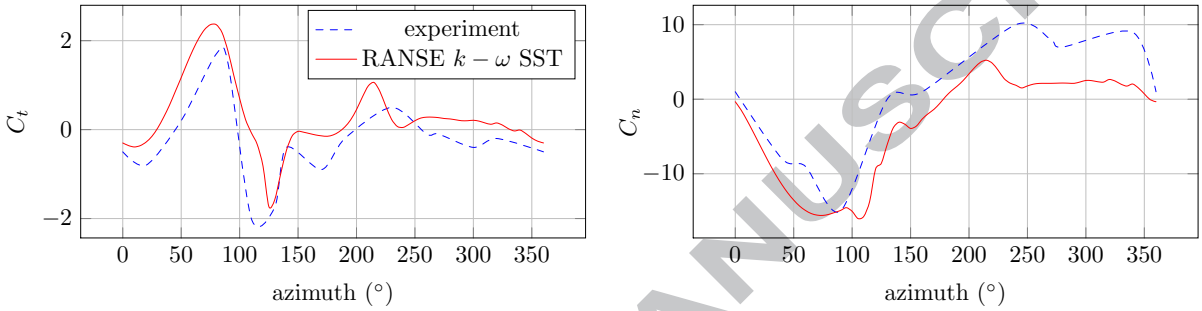

Figure 9: Validation on C_t and C_n for case 4 ($\lambda = 3$, $\sigma = 0.2$)

3.2. Variable pitch

In order to optimize the device, a variable cyclic pitch is added in the computation. The main goal of pitch control are to increase torque and decrease non-productive C_n ; to smooth the forces during the turbine rotation ; and to control cavitation inception.

Sinusoidal pitching was implemented in the present simulation for case 2, $\lambda = 5$. This case was chosen since it has the highest η : .362 (see figure 3). This value is high compared with existing crossflow turbines, for which TSR usually range from 3 to 4 for low solidity turbines [38]. The aim of the present paper is not to provide solution to the pitch law optimization problem, but to validate a model and a workflow. This is why it was not mandatory to choose a nominal λ value.

However, unlike all crossflow wind turbines and most tidal turbines, the targeted configuration of this project is a tidal turbine where holding arms are outside of the water, and the blades are cantilevered. The parasitic arm and junction drag is thus almost cancelled, which enables a turbine λ increase. Even without this feature, recent researches on strut arrangements showed that inclined struts can be beneficial to efficiency [39]. In addition to that, it is believed that multi-objective optimization of the pitch law would result in a nominal λ increase, since main shaft torque, thus generator or gearbox cost would decreased. This would require λ to be a parameter of the optimization, which is outside the scope of this paper.

Three frequencies were tested, namely the first, second and third harmonics, corresponding respectively to

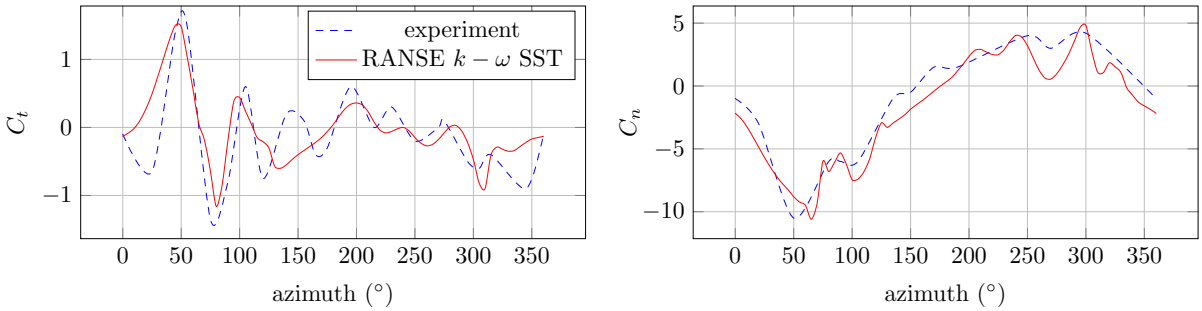

Figure 10: Validation on C_t and C_n for case 5 ($\lambda = 1.5$, $\sigma = 0.1$)

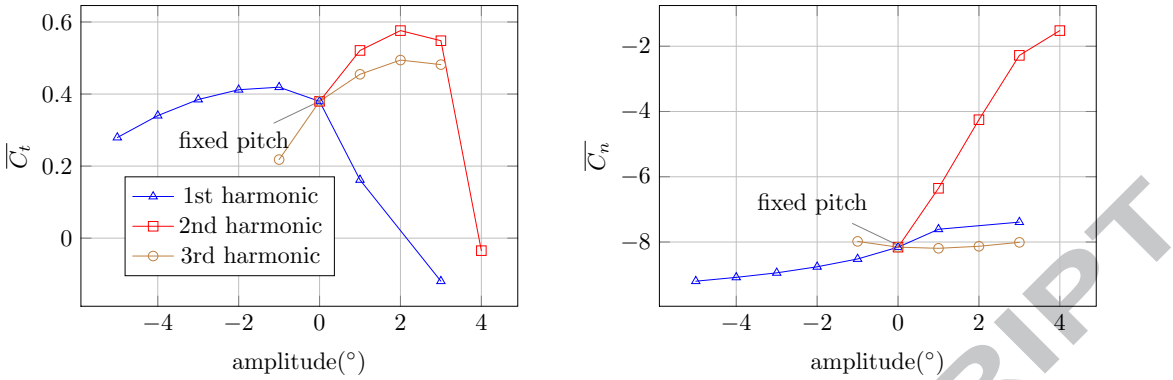

Figure 11: Influence of pitch function amplitude on $\overline{C_t}$ and $\overline{C_n}$

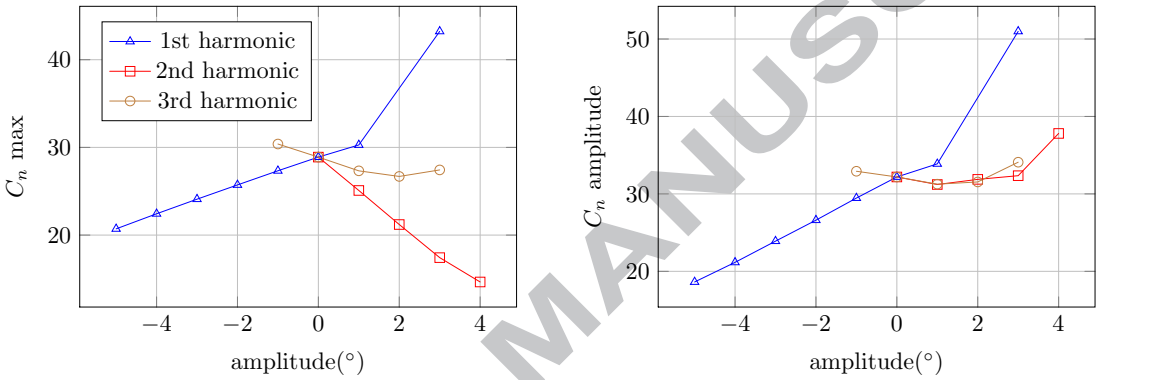

Figure 12: Influence of pitch function amplitude on maximum and amplitude value of C_n

the turbine frequency, twice the turbine frequency and three times the turbine frequency. Various amplitudes from -5° to 4° were tested for each frequency.

3.2.1. Performance study

Mean forces coefficients as a function of pitch amplitude and frequency are displayed on figure 11. Fixed pitch is displayed as a zero amplitude function. As observed, the second harmonic function shows the best results. The best η is obtained for an amplitude of 2° with an increase of 52% in tangential force, in addition to a decrease of 49% in normal force. An amplitude of 3° gives almost the same performance, with a further 50% decrease in normal force.

Maximum and amplitude values of normal force coefficient are shown in figure 12. A large reduction can be obtained on the maximum value with the second order functions, which will decrease the ultimate load. However the amplitude load remains almost constant below an amplitude of 3°. The C_n reduction in upstream part results in an increase downstream. This pitch control strategy will not decrease vibratory or fatigue constraints.

3.2.2. Pitch angle influence on unsteady C_t

The best pitch functions for each harmonic are closely studied now. f1a-2 stands for the first harmonic function with an amplitude of -2°, $\beta_{f1a-2} = -2\sin(\omega t)$; f2a2 stands for the second harmonic function with an amplitude of +2°, $\beta_{f2a2} = 2(\cos(2\omega t) - 1)$ (notice the -1, required to reach 0° at upstream-downstream transitions. It yields a minimum incidence of -4°, not 2°) ; f3a3 stands for the third harmonic function with an amplitude of +3°, $\beta_{f3a3} = 3\sin(3\omega t)$. These functions are shown figure 13, where $\theta = \omega t$. Positive pitch angles stand for an inward rotation of the leading edge.

Absolute difference between C_t with fixed and variable pitch is shown in figure 14. Both f1a-2 and f2a2 exhibit similar behavior on the upstream part. C_t is increased at the beginning of the upstream section, and after 40° the difference decreases, and becomes negative for f2a2. At 85° it starts increasing again, and both functions give the most increase for upstream part at 135°. For f3a3 the steep rise in pitch at the start and end of the upstream part decreases the tangential load. For the downstream part, performance is improved

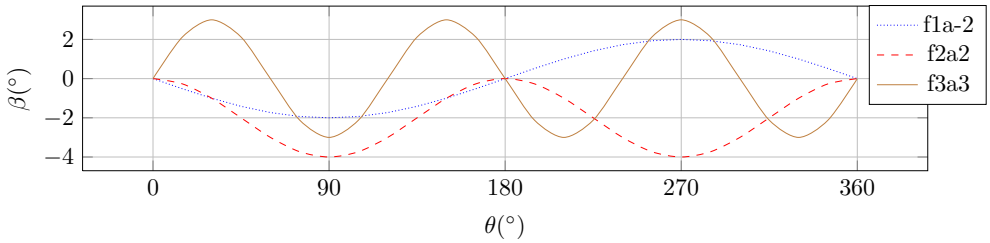

Figure 13: Sinusoidal pitch functions $\beta(\theta)$

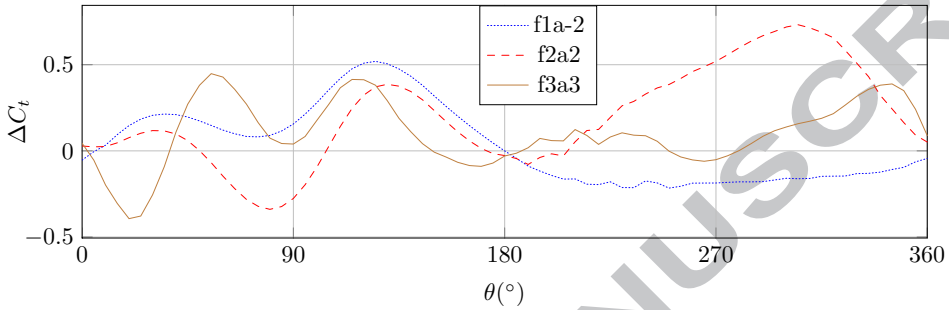

Figure 14: Difference in C_t for variable pitch compared with fixed pitch

for all pitch functions when pitch angle is decreased, thus increasing the angle of attack. This figure leads to several conclusions. First increasing incidence on the upstream part is disadvantageous for this regime, and a decrease of -2° in pitch looks optimal. Second, decreasing pitch below -2° is not beneficial as shown for f2a2 for which minimum pitch is -4°. Third an incidence increase on downstream part is beneficial, which is due to flow deceleration. The strong coupling between local incidence, local flow velocity and pitch angle function requires further investigation on flow deceleration.

3.2.3. Flow velocity reduction

A tidal turbine converts fluid kinetic energy into solid rotational kinetic energy. The amount of reduction in flow velocity occurring when the fluid travels through the turbine is crucial. A small reduction results in a low transfer between fluid and solid. A large reduction results in much energy being withdrawn from the fluid, but not necessarily transferred to the solid, and can create undesirable high disturbance in the flow. According to the momentum theory, the energy extraction is maximum when the flow velocity downstream of the turbine is one third of the upstream flow velocity [40].

The overall reduction can be illustrated by the axial velocity reduction along the axial centerline, shown figure 15. All pitch functions reduce the angle of attack at upstream part, thus reducing flow disturbance and inducing a faster upstream flow velocity compared with fixed pitch. On downstream part f2a2 is the only function for which flow is decelerated below fixed pitch values. Indeed, $\beta_{f2a2} < 0$ for all θ unlike the others laws, resulting in f2a2 being the only function increasing angle of attack everywhere downstream. The other two functions show faster flow. f3a3 is the function creating fastest flow on the central axis of the turbine. A slight velocity increase is observed downstream. This can be explained by the fast rotation of the blade around its quarter chord, creating a propelling effect on the flow. Another conclusion arises from the comparison between f1a-2 and f2a2. On upstream part these functions create very similar deceleration, despite f2a2 reaching a pitch of -4° and f1a-2 reaching -2°. The least flow disturbance by f2a2 should result in a faster flow, however the high incidence at downstream part also disturbs the upstream part. This shows how crucial the correlation between upstream and downstream functions is, and why the flow velocity variation needs to be precisely assessed.

3.2.4. Pressure field

The pressure fields compared between fixed and variable pitch around one blade are shown in figure 16. For case 2, figure 16a, the pressure on the upstream part remains quite low and constant at the suction side between $\theta = 40°$ and 120°. The low pressure area is much smaller on the downstream part however. This is due to the velocity reduction induced by the upstream part, which reduces the angle of attack.

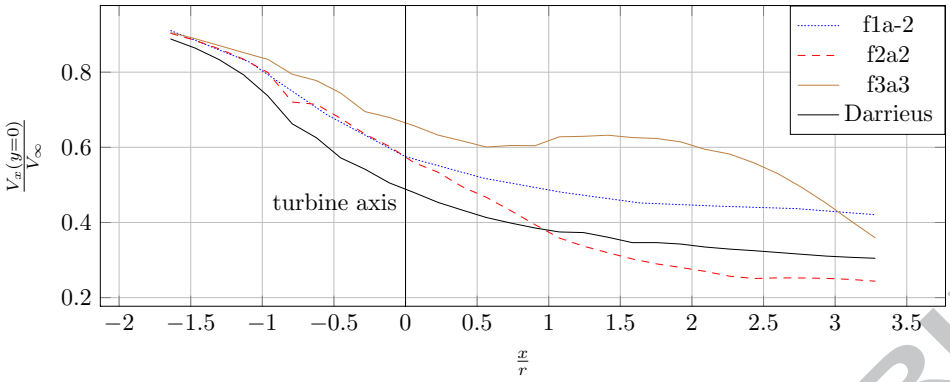

Figure 15: Flow deceleration through turbine center

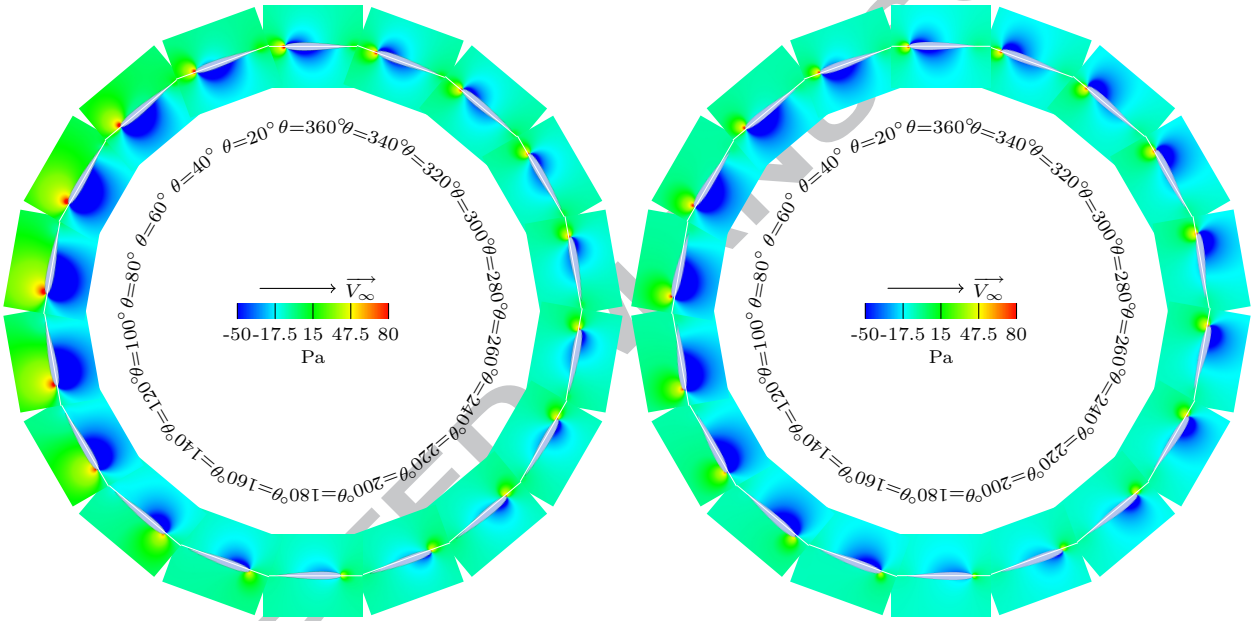

(a) Case 2, $\lambda = 5$

(b) variable pitch Darrieus, $\lambda = 5$

Figure 16: Pressure field

The tangential and normal force coefficient (figure 7) are thus much smaller for the downstream part. For variable pitch, figure 16b, the law considered is the optimal for this study, f2a2. The low pressure at the suction side is weaker at the upstream part, and stronger at the downstream part. This results in a more levelled and better energy conversion. The upstream part extracts less power, which means power can be extracted more efficiently from the downstream part.

3.2.5. Axial velocity field

The axial velocity fields compared between fixed and variable pitch are shown in figure 17. The axial rather than the transverse component or the magnitude was chosen, since it is the energy source from which the turbine can produce power. Fixed pitch is shown in figure 17a, and variable pitch f2a2 is shown in figure 17b. The first difference observed is the wake at the transition between upstream and downstream parts, top and bottom parts of the illustrations. With fixed pitch the blades create a wake where flow velocity is increased, which translates into energy loss. A different pitch angle could result in better efficiency. On the other hand with variable pitch f2a2, this wake is reduced greatly. This pitch law enables the blades to go through zero angle of attack at a better azimuthal position during the transition where pressure and suction side are reversed. The flow velocity reduction due to energy conversion is clearly visible for all angles. It is thus obvious that during the downstream pass, the blade moves in a much slower fluid, and hence has much lower energy available for conversion, which results in lower tangential force coefficient and torque.

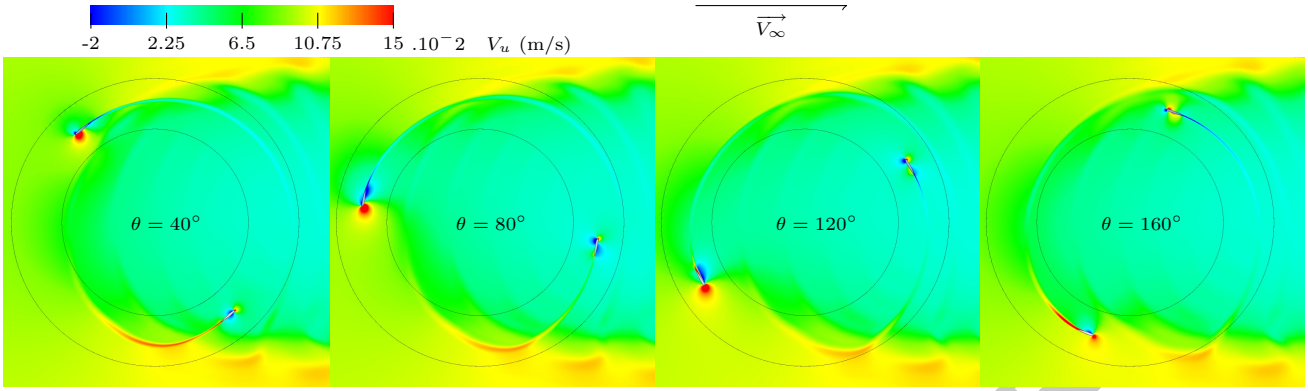

(a) Case 2, $\lambda = 5$

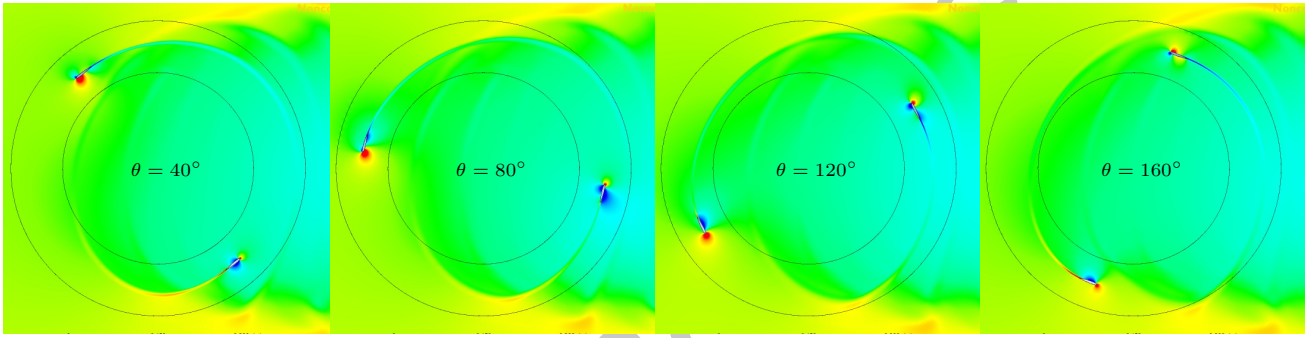

(b) variable pitch Darrieus, $\lambda = 5$

Figure 17: Axial velocity field

3.2.6. Chordwise pressure coefficient distribution

Pressure coefficient C_p along blade boundary is shown figure 18. The x coordinate is the adimensional chord position, and the curves are given for several azimuthal positions. The pitch functions are drawn along the θ axis at the bottom right of the chart. A circle on each curve indicates the outer part of the turbine. The fixed pitch case and the three pitch functions introduced earlier are shown. The fixed pitch turbine creates a lower minimum C_p than variable pitch, hence higher cavitation sensitivity. The higher incidence of f3a3 at the beginning and end of the upstream section translate into two slightly smaller peaks. For the fixed pitch, f1a-2 and f3a3, plateaux can be noticed. They are the sign of stall inception through vortex formation. These plateaux remains quite thin, which means complete stall is avoided. However these C_p singularities create disturbance in the flow which should be avoided. f2a2 shows no sign of stall, and its lower C_p peak would result in lower cavitation sensitivity. On the downstream part however, the higher angle of attack associated with f2a2 results in a higher C_p peak, with a maximum value equal to the maximum upstream value. Again, this means that a more levelled energy extraction is obtained with this law. f2a2 creates a much greater suction at the downstream part. It is the main reason for its higher performance. It can finally be noticed that the curves shown between 220° and 340° are very different from a pitching blade, with a C_p lower on the intrados than on the extrados on the rear part of the blade. This illustrates the flow curvature effect and is consistent with previous studies [41, 42].

3.2.7. Energy consumption of pitch control

The torque required to set the blades in motion results in additional energy transfer and needs to be assessed. The comparison between the energy extracted by the device and this pitch moment energy is carried out by reducing the power needed to drive the pitch to a value dimensionally equivalent to the performance coefficient η, defined as η_β. It is negative when power is needed to set the blades in motion, hence reducing the global performance. Hydrodynamic moment on blades M_{hydro} is given by URANSE computation. η_β is then computed by the following equation : $\eta_\beta = \frac{M_{\text{hydro}}\dot{\beta}}{\frac{1}{2}\rho 2rlv_\infty^3}$

Two approaches can be used to assess this influence. If a mechanical device, or a hydraulic device is used to obtain pitch variation, then when η_β is positive, additional power can be fed back to the primary power extraction. This is not true when servomotors are used, and in this case only negative values of

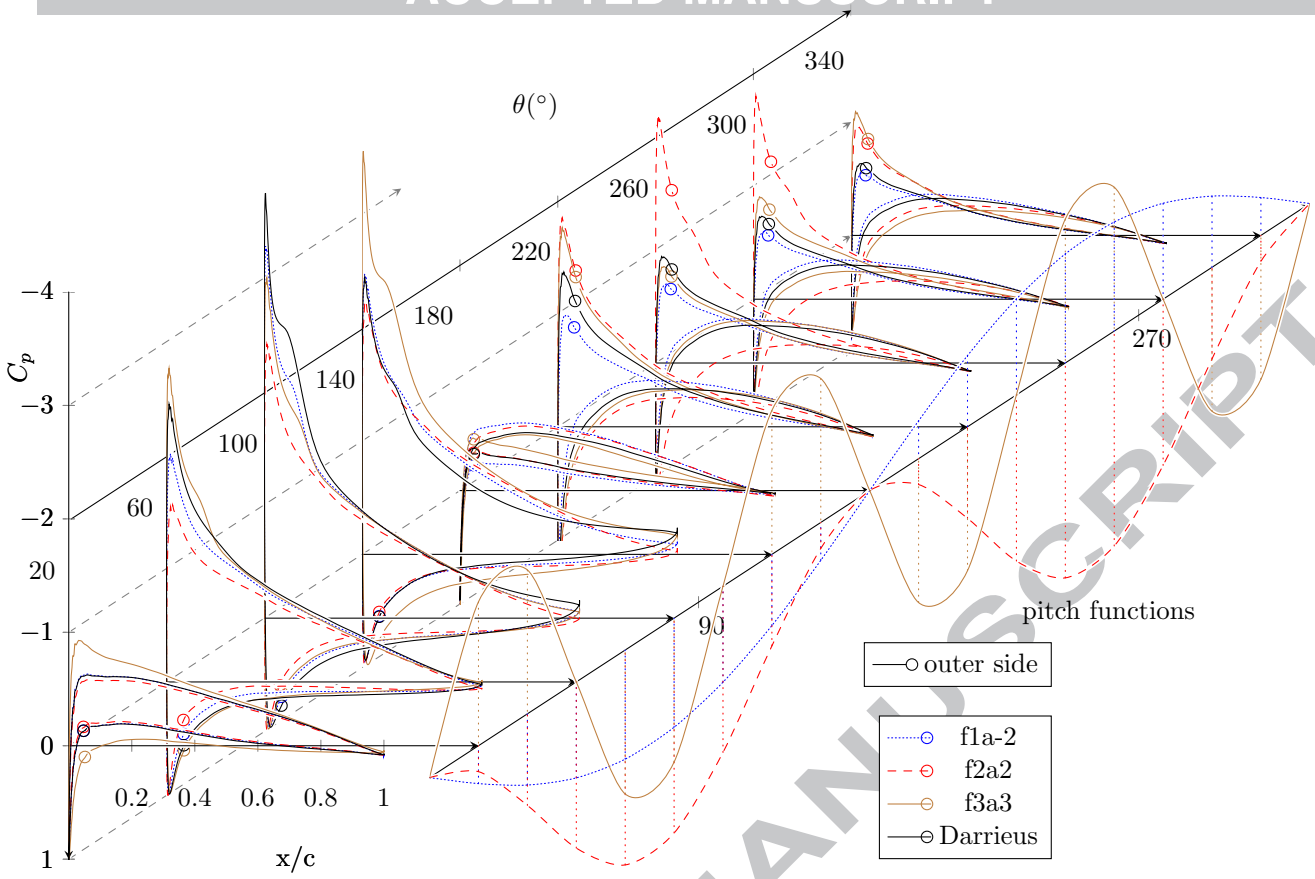

Figure 18: Pressure coefficient for f1a-2, f2a2, f3a3

loi	η (%)	η_β	η_β with negative values
Darrieus	28,45	-	-
f2a1	39,03	0,20	-0,29
f2a2	43,16	0,49	-0,47
f2a3	41,06	0,71	-0,66
f2a4	-2,60	-1,14	-2,64
f3a1	34,07	0,05	-0,73
f3a2	37,03	0,04	-1,52
f3a3	36,09	-0,08	-2,38

Table 5: Global and moment performance coefficients

η_β need to be considered. Results for f2 and f3 can be found in table 5. For the approach consisting of averaging all the values, the moment performance coefficient is mainly positive. f2a2 would benefit from an additional 0.49% in η. Only f3a3 would get a negative value of only 0.08% which is very low. When using only negative values, f3a3 would have its performance decreased by 2.38%, f2a2 by 0.47%. The higher moment influence on f3 functions is explained by a faster pitch velocity. The third harmonics are thus less desirable for further studies. The hydrodynamic moment associated with lift generation is considered here at quarter chord. For energy consumption reduction this location may be optimized, which is outside the scope of this work. It was however important to demonstrate that, even with the quarter chord as pitch center, the energy consumption remains very low compared with the gain associated with active variable pitch.

4. Conclusion

The simulation of a cross-flow turbine has been implemented in a URANSE solver. The validation of the model is based on the comparison with experimental data obtained from the literature. The validation against experimental data was performed on the tangential and normal force comparison for five configurations corresponding to various tip speed ratios and solidities. The computation is based on the fully

turbulent $k\omega$ SST model. However because of moderate chord length Reynolds number in the experiments, a transition model was also tested. The computation domain was built with a rotating ring containing blades, enclosed inside a steady domain with sliding interfaces at the boundaries. The boundary layer could thus be meshed with high quality, independently of the turbine rotation. Thorough determination of simulation parameters and discretizations has been carried out and shows that a 1° discretization of the turbine rotation is necessary, that y+ has to be lower than unity to correctly compute the boundary layer close to the foil surface, and that 300 cells are required in the chordwise direction along the blades. It is observed that the agreement is rather good for all cases for the fully turbulent model. Even though the experimental forces results led the author to believe transition might have occurred, it could not be obtained with the $\gamma - Re_\theta$ transition model. The complexity associated with the upstream-downstream interaction is found to be the main source of discrepancies. The close analysis of wall pressure coefficient and flow field at various stages of the turbine rotation highlights boundary layer events such as separation, stall, vortex shedding and flow reattachment. This allows the authors to believe that the present simulation is accurate enough to be used for the simulation of variable pitch cross-flow turbines. With such devices flow events can be controlled and power production can be optimized with the use of sinusoidal pitch functions, by varying the frequency and amplitude. Variable pitch was implemented for a tip speed ratio of 5, aiming at performance improvement primarily. Sinusoidal functions of different orders were tested. The second harmonic functions resulted in a performance increase of 52%. For this regime optimal pitch variation seems to require a very slight recirculation and an incidence decrease on upstream section, and an angle of attack increase on downstream section. The flow deceleration through the turbine was found to be a primary factor in pitch function performance evaluation. Finally the power required to set blades into motion around their quarter chord was compared with the power extracted by the turbine. The ratio was found to be lower than 3% for third harmonics, and lower than 0.5% for second order harmonics. The performance gain associated with variable sinusoidal pitch control is thus relevant for further study and optimization. The future steps consists in the assessment of composed sinusoidal pitch functions ; the addition of a pitch offset ; the analysis of the pitch center location ; the addition of λ as an optimization parameter ; the evaluation in inclusion of arm and junction drag in the optimization ; and finally the computation and optimization of arbitrary pitch functions.

References

[1] MJ Khan, G. Bhuyan, MT Iqbal, and JE Quaicoe. Hydrokinetic energy conversion systems and assessment of horizontal and vertical axis turbines for river and tidal applications: A technology status review. *Applied Energy*, 86(10):1823–1835, 2009.

[2] S. Kiho, M. Shiono, and K. Suzuki. The power generation from tidal currents by darrieus turbine. *Renewable energy*, 9(1-4):1242–1245, 1996.

[3] J. Zanette, D. Imbault, and A. Tourabi. A design methodology for cross flow water turbines. *Renewable Energy*, 35(5):997–1009, 2010.

[4] BK Kirke and L. Lazauskas. Limitations of fixed pitch darrieus hydrokinetic turbines and the challenge of variable pitch. *Renewable Energy*, 36:893–897, 2010.

[5] B. Paillard, F. Hauville, and J.A. Astolfi. Evaluation of active variable pitch technologies as current turbines. In *World Renewable Energy Congress*, 2008.

[6] Benoit Paillard, Jacques-Andre Astolfi, and Frederic Hauville. Cfd simulation and experimental validation of a vertical axis turbine: Toward variable pitch cross-flow marine turbine for maximizing hydropower extraction the shiva project. In *OMAE*. ASME, 2011.

[7] Benoit Paillard. *Simulation numérique et optimisation d'une hydrolienne à axe transverse avec contrôle actif de l'angle de calage*. PhD thesis, IRENAV, 2011.

[8] B Paillard, F Hauville, and JA Astolfi. Simulating variable pitch crossflow water turbines: A coupled unsteady onera-edlin model and streamtube model. *Renewable Energy*, 52:209–217, 2013.

[9] CJ Simão Ferreira. *The near wake of the VAWT, 2D and 3D views of the VAWT aerodynamics*. PhD thesis, PhD Thesis, Delft University of Technology, Delft, the Nederlands, 2009.

[10] A Allet, S Hallé, and I Paraschivoiu. Numerical simulation of dynamic stall around an airfoil in darrieus motion. *Journal of solar energy engineering*, 121(1):69–76, 1999.

[11] CJ Ferreira, H. Bijl, G. Bussel, and G. Kuik. Simulating dynamic stall in a 2d vawt: Modeling strategy, verification and validation with particle image velocimetry data. In *Journal of Physics: Conference Series*, volume 75, page 012023. IOP Publishing, 2007.

[12] CA Consul, RHJ Willden, E. Ferrer, and MD McCulloch. Influence of solidity on the performance of a cross-flow turbine. In *8th European Wave and Tidal Energy Conference, Uppsala, Sweden*, 2009.

[13] VR Klaptocz, GW Rawlings, Y. Nabavi, M. Alidadi, Y. Li, and SM Calisal. Numerical and Experimental Investigation of a Ducted Vertical Axis Tidal Current Turbine. In *Proceedings of the 7th European Wave and Tidal Energy Conference, Porto, Portugal*, 2007.

[14] S. Antheaume, T. Maître, and J.L. Achard. Hydraulic darrieus turbines efficiency for free fluid flow conditions versus power farms conditions. *Renewable Energy*, 33(10):2186–2198, 2008.

[15] DP Coiro, F. Nicolosi, A. De Marco, S. Melon, and F. Montella. Dynamic behavior of novel vertical axis tidal current turbine: numerical and experimental investigations. In *ISOPE-2005: Fifteenth(2005) International Offshore and Offshore*

and Polar Engineering Conference, volume 1, page 4. International Society of Offshore and Polar Engineers, P. O. Box 189, Cupertino, CA, 95015-0189, USA,, 2005.

[16] JJ Miau, SY Liang, RM Yu, CC Hu, TS Leu, JC Cheng, and SJ Chen. Design and test of a vertical-axis wind turbine with pitch control. *Applied Mechanics and Materials*, 225:338–343, 2012.

[17] I.S. Hwang, Y.H. Lee, and S.J. Kim. Optimization of cycloidal water turbine and the performance improvement by individual blade control. *Applied Energy*, 86(9):1532–1540, 2009.

[18] W. Grylls, B. Dale, and PE Sarre. A theoretical and experimental investigation into the variable pitch vertical axis wind turbine. In *Second International Symposium on Wind Energy Systems, Amsterdam, NetherlandsE*, volume 9, 1978.

[19] V. Nattuvetty and WW Gunkel. Theoretical performance of a straight-bladed cycloturbine under four different operating conditions. *Wind Engineering*, 6(3):110–130, 1982.

[20] DW Erickson, JJ Wallace, and Jaime Peraire. Performance characterization of cyclic blade pitch variation on a vertical axis wind turbine. *Aerospace Sciences Meeting including the New Horizons Forum and Aerospace Exposition*, 2011.

[21] JW Anderson, RV Brulle, EB Birchfield, and WD Duwe. Mcdonnell 40-kw giromill wind system: Phase i-design and analysis. volume ii. technical report. Technical report, Rockwell International Corp., Golden, CO (USA). Rocky Flats Plant; McDonnell Aircraft Co., St. Louis, MO (USA), 1979.

[22] D. Vandenberghe and E. Dick. Optimum pitch control for vertical axis wind turbines. *Wind Engineering*, 11(5):237–247, 1987.

[23] F. Kaare and E. Evensen. Turbine driven with a fluid medium, April 26 2005. US Patent 6,884,020.

[24] A. Ducoin. *Etude experimentale et numerique du chargement hydrodynamique des corps portants en regime transitoire avec prise en compte du couplage fluide structure*. PhD thesis, IRENav, 2008.

[25] JH Strickland, BT Webster, and T. Nguyen. A vortex model of the Darrieus turbine: An analytical and experimental study. *Journal of Fluids Engineering*, 101:500–505, 1979.

[26] P. Vittecoq and A. Laneville. Etude en soufflerie d'un rotor de type Darrieus. Technical Report Rept. MEC-82-2, Mechanical Engineering Department, University of Sherbrooke, Quebec, Canada, August 1982.

[27] ANSYS. *ANSYS CFX-Solver Theory Guide*. ANSYS, Inc., Southpointe 275 Technology Drive Canonsburg, PA 15317, December 2006.

[28] D Bouris and G Bergeles. 2d les of vortex shedding from a square cylinder. *Journal of Wind Engineering and Industrial Aerodynamics*, 80(1):31–46, 1999.

[29] E. Amet. *Simulation numérique d'une hydrolienne à axe vertical de type Darrieus*. PhD thesis, Institut polytechnique de Grenoble & Université Technique de Constructions de Bucarest, 2009.

[30] FR Menter, R. Langtry, and S. V
"olker. Transition modelling for general purpose cfd codes. *Flow, turbulence and combustion*, 77(1):277–303, 2006.

[31] Robert H Liebeck. A class of airfoils designed for high lift in incompressible flow. *Journal of Aircraft*, 10(10):610–617, 1973.

[32] A. Ducoin, F. Deniset, J.A. Astolfi, and J.F. Sigrist. Numerical and experimental investigation of hydrodynamic characteristics of deformable hydrofoils. *Journal of Ship Research*, 53(4):214–226, 2009.

[33] FR Menter, RB Langtry, SR Likki, YB Suzen, PG Huang, and S. V
"olker. A correlation-based transition model using local variables part i: model formulation. *Journal of Turbomachinery*, 128:413, 2006.

[34] PL Delafin, F Deniset, and JA Astolfi. Effect of the laminar separation bubble induced transition on the hydrodynamic performance of a hydrofoil. *European Journal of Mechanics-B/Fluids*, 46:190–200, 2014.

[35] Pl Delafin, François Deniset, Jacques-André Astolfi, Jean-Marc Laurens, et al. Prediction of hydrodynamic forces with and without transition model. In *NuTTS*, 2012.

[36] Paul C Klimas and Mark H Worstell. Effects of blade preset pitch/offset on curved-blade darrieus vertical axis wind turbine performance. Technical report, Sandia National Labs., Albuquerque, NM (USA), 1981.

[37] Andrzej Fiedler. The effects of blade pitch and mount point offset on vertical axis wind turbine performance. Master's thesis, McMaster University, 2009.

[38] I. Paraschivoiu. *Wind Turbine Design: With Emphasis on Darrieus Concept*. Polytechnic International Press, Canada, 2002.

[39] Agostino De Marco, Domenico P Coiro, Domenico Cucco, and Fabrizio Nicolosi. A numerical study on a vertical-axis wind turbine with inclined arms. *International Journal of Aerospace Engineering*, 2014, 2014.

[40] Albert Betz. *Introduction to the theory of flow machines*. Pergamon, 1966.

[41] José L Cardona. Flow curvature and dynamic stall simulated with an aerodynamic free-vortex model for vawt. *Wind Engineering*, 8:135–143, 1984.

[42] Domenico Coiro, Fabrizio Nicolosi, Agostino De Marco, Stefano Melone, and Francesco Montella. Flow curvature effect on dynamic behaviour of a novel vertical axis tidal current turbine: Numerical and experimental analysis. In *ASME 2005 24th International Conference on Offshore Mechanics and Arctic Engineering*, pages 601–609. American Society of Mechanical Engineers, 2005.

RANS modelization of a Darrieus crossflow turbine where blades' pitch angle changes over time to improve performance > Complete validation on a fixed pitch system, with models comparison and temporal/spatial discretization study > Influence of periodical pitch variation on performance including power required for pitch variation > Local pressure coefficient description